Frontiers in Heat and Mass Transfer

Tech Science Press

https://doi.org/10.32604/fhmt.2026.075814

REVIEW

Review on the Optimal Design of Cyclone Separator: Theory, Methodology, and Applications

Bin Li[1,2], Liying Gao[1,2,*], Yong Li[3], Kun Zhu[1,2], Zhenling Fu[1,2], Shifan Xu[1,2] and Mohan Li[1,2]

[1]School of Mechanical Engineering, Shandong Key Laboratory of CNC Machine Tool Functional Components, Qilu University of Technology (Shandong Academy of Sciences), Jinan, China
[2]Shandong Institute of Mechanical Design and Research, Jinan, China
[3]School of Mechanical Engineering, University of Jinan, Jinan, China

*Corresponding Author: Liying Gao. Email: gly@qlu.edu.cn

Received: 09 November 2025; Accepted: 16 January 2026; Published: 29 June 2026

ABSTRACT: Cyclone separators are highly efficient gas-solid separation that operate on the centrifugal force and play an indispensable role in industries such as chemical engineering, environmental protection, and power generation. They exhibit excellent reliability, particularly under demanding conditions such as high temperatures and elevated particle concentrations. However, a persistent trade-off between separation efficiency and pressure drop has limited further performance improvements. To address this, optimization of cyclone separators has become a major research focus. This article systematically reviews recent advances, first by examining the mechanisms through which key structural parameters, such as inlet geometry, exhaust pipe diameter, and cone angle, influence performance across different industrial applications. Furthermore, the review introduces an integrated optimization framework based on computational fluid dynamics (CFD) simulations, surrogate modelling, and intelligent optimization algorithms to enhance design performance. It critically compares the applicability and limitations of various high-dimensional optimization methods and their integration strategies. The article underscores a paradigm shift from optimizing instantaneous performance toward establishing a lifecycle optimization (LCO) framework that incorporates long-term metrics such as wear and maintenance costs. Evidence shows that coupling CFD with intelligent algorithms enables efficient exploration of multi-objective parameter spaces. Finally, the article discusses current limitations in optimization research and outlines future directions, including multi-physics coupling involving flow, heat, and particle transport, lifecycle optimization, and intelligent decision support systems. In summary, this review establishes a theoretical foundation and provides technical guidance for the energy-efficient, high-performance design and industrial implementation of cyclone separators.

KEYWORDS: Cyclone separator; CFD; surrogate model; heat transfer; intelligent optimization algorithm

1 Introduction

Cyclone separators are widely used in industries ranging from petrochemical catalyst recovery [1] and pharmaceuticals [2] to mineral processing [3], industrial mitigation [4], and circulating fluidized bed boilers [5]. Which are play a critical role under harsh operating conditions, such as elevated temperatures and high particle loadings, by maintaining plant reliability and preventing equipment damage. Cyclone separators achieve efficient gas-solid phase separation through the centrifugal force generated by high-speed rotating airflow. In petroleum catalytic cracking units, they quickly separate high-temperature catalyst

particles from the reaction oil and gas, preventing blockages or wear in downstream equipment [6]. In coal-fired boiler systems, they effectively remove high-concentration fly ash, reducing flue gas dust content and alleviating the dust removal load on subsequent systems, thus protecting key equipment such as fans [7]. The lack of moving parts, tolerance to high temperatures and inherently stable geometry make cyclones low-maintenance, robust separators that sustain high performance even in extreme service conditions.

Cyclone separators typically employ a single volute inlet and a fixed conical geometry [8], but this design struggles to reconcile high separation η with low energy consumption [9]. Specifically, increasing the inlet velocity can enhance centrifugal force and improve η, but it also results in a substantial increase in ΔP, leading to a significant rise in energy consumption [10]. Conversely, reducing ΔP weakens the centrifugal force, which negatively impacts η of fine particles [11]. To address these limitations, optimization design methods have been developed to enhance the performance of cyclone separators. Optimization aims to achieve an optimal match between geometric configuration and performance through systematic analysis and parameter tuning [12]. Optimizing cyclone separators requires coordinated tuning of inlet, body, and outlet geometries [13] to lower ΔP without compromising η, thus reducing energy consumption.

A combination of experimental testing, numerical simulation and theoretical modeling is commonly employed in cyclone optimization design. Experimental work provides direct validation of key performance metrics such as η and ΔP but also has important limitations. Experiments are costly and require bespoke test rigs, which often lead to long iteration cycles. For example, an industrial comparison by Xie et al. [14] required more than six months of research and development. Data coverage is particularly limited for fine particles smaller than 5 μm. Zhang et al. [15] reported a sharp decline in capture efficiency for particles below 5 μm, with measured values falling under 70, and they also noted significant measurement uncertainty because the impact sampler produced counting errors of up to ±18% in the 0.1 to 1 μm range. Experiments are also poorly suited to capturing transient flow phenomena such as turbulent pulsations and backflow. High-fidelity numerical approaches, notably large eddy simulation, can resolve these rapid dynamic structures, as demonstrated by Erol et al. [16]. These complementary strengths and weaknesses have encouraged a transition toward simulation-driven workflows and intelligent optimization algorithms and have motivated the development of integrated frameworks that combine experiments, physics-based simulations and algorithmic optimization.

This paper presents a comprehensive review of recent progress in the parameter optimization of cyclone separators, with particular emphasis on integrated optimization frameworks that combine CFD simulations, surrogate modeling, and intelligent optimization algorithms to improve η and reduce ΔP. The review analyzes the influence of key geometric parameters, including vortex finder diameter, inlet configuration, and cone angle, on cyclone performance. It also discusses the differing performance requirements among industrial sectors such as chemical processing, environmental protection, and power generation, and assesses the applicability and limitations of various optimization strategies, including multi-objective evolutionary algorithms. This review aims to provide a solid theoretical basis and a practical methodological framework to guide the precise design and industrial implementation of cyclone separators.

2 Fundamentals of Cyclone Separator Parameter Optimization

The cyclone separator consists of several main components, including the air inlet, exhaust pipe, dust outlet, and the separator body [17]. The structural parameters of the cyclone are illustrated in Fig. 1. Among these parameters, the exhaust pipe diameter (D_x) has the greatest influence on both ΔP and η [18]. Other important parameters that affect performance include the inlet length (L_i), cone angle (θ), inlet height (a), inlet width (b), total separator length (H), exhaust pipe insertion depth (S), and the cone bottom diameter

(B_c) [8]. Together, these geometric factors govern the flow structure and directly determine the balance between energy consumption and η.

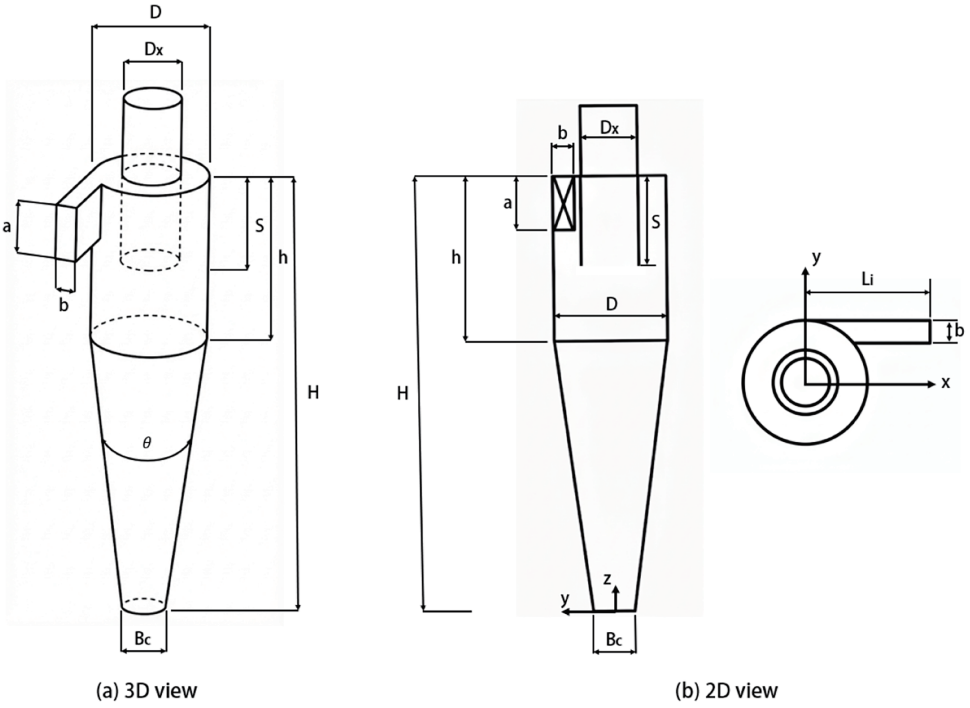

Figure 1: Schematic diagram for cyclone separator.

The optimization of cyclone separators primarily focuses on two core objectives: ΔP and η. These factors have a decisive influence on the overall performance of the equipment [19]. η, as a critical metric for assessing gas-solid separation capabilities, not only determines whether process emissions comply with environmental standards and prevents particle wear or blockage in downstream equipment, but also influences material recovery efficiency. It is essential for ensuring the practical viability of the equipment [20]. In contrast, the pressure drop reflects the energy loss of the gas flow through the separator. Excessive ΔP increases the power consumption of the driving equipment, elevates operational costs, and may disturb the airflow balance between upstream and downstream units, thereby compromising system stability [21]. The relationship between η and ΔP presents a clear trade-off. Therefore, the optimization process must balance ΔP control with the required η, or enhance efficiency within an acceptable ΔP range, to achieve the best compromise between performance and energy consumption.

2.1 Key Parameters of Cyclone Separator and Their Impact

In cyclone separator design, overall performance and operational stability largely depend on the coordinated interaction among key structural parameters and geometric features.

2.1.1 Analysis of Key Structural Parameters

(1) Impact of inlet angle on performance

In fluid catalytic cracking units, the performance of cyclone separators has a direct impact on catalyst recovery efficiency and the overall operating economy. Bernardo et al. [22] investigated the effect of a modified cyclone design featuring a 45 inclined inlet using CFD simulations. The results showed that at an

inlet velocity of 2.75 m/s, the inclined inlet design led to a tangential velocity peak approximately twice that of the conventional design. This increase in tangential velocity brought the high-speed vortex region closer to the inner wall, thereby enhancing the centrifugal force and promoting particle deposition on the wall, which improved separation efficiency. Additionally, the study reduced the tangential velocity peak in the gas-solid two-phase flow by approximately 50%, significantly lowering ΔP while maintaining high η.

(2) Influence of the length of the cylinder and cone structure

In the petrochemical technology, energy and power engineering industries, Stairmand high-efficiency cyclone separators are widely used for gas-solid separation. Enhancing their performance is crucial for reducing system energy consumption and improving η. Brar et al. [23] used CFD simulations to investigate the effects of cylinder and cone length on cyclone performance. The results showed that at an inlet velocity of 16.1 m/s, increasing the cylinder length to 5.5 times the cyclone diameter reduced ΔP by approximately 34% and improved η by 9.72%. Similarly, extending the cone length to 6.5 times the diameter lowered the ΔP by about 29% and increased η by 10.8%.

(3) Selection of inlet structural forms and adaptation to application scenarios

The inlet structure plays a critical role in shaping the flow field and determining the energy consumption of a cyclone separator. In industrial applications, the combination of an axial inlet and guide vanes is widely adopted. The guide vanes regulate the swirl intensity, reducing turbulence to below 15% and lowering ΔP by 20%–30% compared with conventional tangential inlets [24]. In high dust concentration environments, such as cement grinding systems where the dust mass concentration exceeds 500 g/m^3, a tangential inlet with an aspect ratio of 1:2 to 1:3 is typically employed. This design enlarges the inlet area by approximately 40% relative to standard inlets while maintaining an inlet velocity between 18 and 25 m/s. This configuration not only ensures the maintenance of a strong swirl field but also prevents particle agglomeration and blockage. Studies have demonstrated that this design can raise the centrifugal acceleration of particles larger than 5 μm to over 500 m/s^2, thereby significantly improving separation efficiency. In addition, extending the inlet height improves particle residence time and helps suppress back mixing phenomena [25].

(4) Key indicators and operating requirements for exhaust pipe parameter design

The exhaust pipe is a critical component governing the escape of fine particles in cyclone separators, with its design primarily determined by the critical escape particle size (d_{crit}) as the core performance indicator. In high-purity applications, such as the pharmaceutical and food industries, the exhaust pipe insertion depth is typically maintained between 1/3 and 1/2 of the cylinder height, while the diameter ratio (B_c/D) is controlled within the range of 0.4 to 0.6. This design suppresses outlet vortices and minimizes the escape of fine particles [26]. This combination of parameters significantly reduces system ΔP and energy consumption while maintaining effective η. The improvement arises from reduced flow resistance due to the larger diameter and the attenuation of outlet vortices enabled by the shallower insertion depth, which together enhance overall cyclone performance.

(5) Optimization of cone angle and dust outlet size and working conditions requirements

The cone angle and dust outlet size directly affect particle sliding behavior and the wear resistance of cyclone separators. The design is particularly critical under high-temperature and highly abrasive conditions, such as those in circulating fluidized bed boilers (T = 800°C–900°C, particle hardness ≥ 6 Mohs). In these environments, a gentler cone angle of 20°–25° is often used together with a larger dust outlet diameter (B_c/D = 0.3–0.4). This combination reduces the particle impact velocity to 15 m/s, thereby mitigating erosion. Furthermore, lining the equipment with highly wear-resistant materials such as ZGMn13 can limit the wear rate to below 0.1 mm/kh, significantly extending the service life of the cyclone [27].

2.1.2 Effect of Structural Design on Flow Field

The performance of a cyclone separator is influenced by multiple factors, arising from the intricate interplay between its internal flow dynamics and external geometry, rather than by a single parameter.

(1) The Stokes number in the flow field

In gas-solid or liquid-solid separation systems, the Stokes number (Stk) is an important dimensionless parameter used to evaluate particle separability. It is defined as the ratio of the particle relaxation time τ_p to the characteristic time of the fluid τ_f [28,29]:

$$Stk = \frac{\tau_p}{\tau_f} = \frac{\rho_p d_{pu_{in}}^2}{18uD}, \tag{1}$$

where τ_p represents the time required for a particle to decelerate to a rest in the fluid, determined by the particle density (ρ_p), diameter (d_p), inlet velocity (u_{in}), and fluid viscosity (μ). The term τ_f denotes the characteristic time for the fluid to traverse the cyclone's cylindrical section with diameter D. When $Stk \geq 0.1$, the inertial force of the particle which is proportional to d_p^2 overcomes the fluid viscosity, and the centrifugal effect becomes dominant in the separation process. Conversely, when Stk is less than 0.1, viscous forces dominate the flow, causing particles to closely follow the fluid streamlines and hindering their separation [30].

Experimental studies have demonstrated that η exhibits a nonlinear dependence on Stk. When $Stk < 0.01$, η is approximately 0, and the particles are fully carried by the mainstream. For instance, the escape rate of PM 2.5 in conventional cyclone separators exceeds 90%. As Stk increases within the range of $0.01 \leq Stk \leq 1$, η rises exponentially with Stk, reaching 80%–90% at $Stk = 1$, which is the typical design range for industrial cyclone separators. When $Stk > 1$, η approaches 100%, but ΔP increases significantly. For example, at $Stk = 10$, ΔP increases by more than 50% [31].

The Stokes number serves as the fundamental criterion for inertial separation, with its critical value of 0.1 representing the threshold for effective particle separation. The design process requires the coordinated optimization of parameters such as particle diameter (d_p), inlet velocity (u_{in}), and separator diameter to ensure that $Stk \geq 0.1$, while balancing ΔP and energy consumption. Quantitative modeling requires the integration of CFD simulations and experimental verification to effectively address the dynamic separation processes under the influence of multiple interacting factors.

The cylinder diameter is a crucial geometric parameter matched to Stk of the target particles. For instance, in chemical catalyst recovery, it is necessary to reduce the cylinder diameter to a range of 300 to 500 mm to increase the rotational flow velocity and centrifugal acceleration. This adjustment effectively enhances Stk, prolongs particle residence time, and improves separation efficiency [32]. In contrast, in mineral processing, where coarse particles with large Stk are separated, the cylinder diameter can be increased to a range of 1 to 2 m. Furthermore, optimizing the aspect ratio (H/D) to extend the settling distance helps suppress turbulent secondary entrainment, enhance processing capacity, and maintain an appropriate Stokes number [33].

(2) The effect of particle Reynolds number on the flow field

When performing simulations in Ansys Fluent, the discrete phase model (DPM) is typically used to calculate the movement and distribution of particles within the fluid. The particle motion Equation [29] is given by:

$$\frac{d\mu_{pi}}{dt} = \frac{18\mu}{\rho_p d_\rho^2}\frac{C_D Re_p}{24}\left(\mu_i - \mu_{pi}\right) + \frac{g_i\left(\rho_p - \rho\right)}{\rho_p}, \tag{2}$$

$$\frac{dx_{pi}}{dt} = u_{in}, \tag{3}$$

where ρ, ρ_p, d_p, and μ represent the fluid density, particle density, particle diameter, and fluid dynamic viscosity, respectively; C_D is the particle drag coefficient; μ_i and μ_{in} are the fluid velocity and particle velocity, respectively; g_i is the acceleration due to gravity in the i direction. The first term on the right-hand side of Eq. (2) represents the drag force per unit mass acting on the particle. The particle Reynolds number is given by:

$$Re_p = \frac{\rho d_p \left|\mu - \mu_p\right|}{\mu}. \tag{4}$$

Studies have shown that at higher Reynolds numbers (e.g., $Re > 2.8 \times 10^5$), stronger turbulent pulsations and large-scale coherent structures, such as single or double helical precessing vortex cores, develop within the flow field. These structures enhance particle diffusion and mixing, which can lead to the re-entrainment of previously separated particles and consequently reduce separation efficiency [34]. At lower Reynolds numbers, the flow field becomes more stable and turbulent pulsations weaken. While this promotes particle sedimentation, it also reduces the flow rate, thereby reducing processing capacity and overall equipment efficiency [35]. Moreover, variations in Reynolds number influence the stability and frequency characteristics of the vortex core, indirectly influencing the separation performance.

Therefore, in practical applications, it is essential to select an appropriate range of Reynolds numbers based on particle characteristics and operating conditions to achieve a balance between η and energy consumption. When determining geometric parameters such as the cylinder diameter, it is crucial to consider the combined effects of both the Stokes number and the Reynolds number. Optimizing these parameters through numerical simulations or experimental validation enables the attainment of an optimal balance between η and processing capacity [32].

The design of gas-solid or liquid-solid separation equipment represents a complex system that requires the coordinated optimization of multiple parameters. This process involves the simultaneous adjustment of key design factors, including cylinder diameter, inlet configuration, exhaust pipe structure, and cone geometry, while accounting for variables such as particle characteristics (Stk), fluid dynamics (Re), and operating conditions. The objective is to achieve a comprehensive optimization that balances η, processing capacity, energy consumption, and operational durability [17].

2.2 Temperature Effects and Heat Transfer Analysis

In industrial processes involving high-temperature particles or flue gas, cyclone separators not only undertake the task of gas-solid separation but have also gradually become important devices for waste-heat recovery [36,37]. As a core operational parameter, temperature exerts a profound influence on η and heat-transfer performance [38] by altering the physical properties of gases and particles [39,40], inducing phase transitions, and affecting fluid dynamic behavior [41,42].

2.2.1 Temperature Effects on Heat Transfer, Waste-Heat Recovery, and Separation Efficiency

(1) Temperature effects on heat transfer and waste-heat recovery performance

Temperature gradients serve as the primary driving force for heat transfer within a cyclone separator. Li et al. [43] illustrates the industrial configuration of the blast-furnace slag waste-heat-recovery system in Fig. 2, including the 60 t/h slag-disposal technology scheme and the associated equipment layout. They investigated waste-heat recovery from molten blast-furnace slag and demonstrated that the rapid self-rotation (up to 14,459 rpm) and orbital motion of particles significantly enhance convective heat transfer between the solid phase and the cooling medium. Consistent observations were made by He et al. [44], who found that intensified particle rotation and turbulent dispersion improve gas-solid thermal exchange and reduce local temperature nonuniformities. Such particle-driven turbulence mechanisms offer an effective route for achieving high-efficiency, intermittent heat recovery from hot solids, potentially leading to substantial net energy gains.

However, higher inlet gas temperatures do not necessarily improve heat-transfer performance. Ma et al. [36] observed that, under a fixed cooling-medium flow rate, the overall heat-transfer efficiency of the cyclone decreased as the flue-gas inlet temperature increased. When the inlet temperature rose from 40°C to 70°C, the maximum heat-transfer efficiency declined sharply (42.1% at the lower condition). This tendency has also been discussed in earlier theoretical and empirical studies by Székely and Carr [45] and Zhu et al. [46], where elevated gas-side temperatures were shown to increase thermal resistance and reduce the overall heat-transfer coefficient due to the weakening of the temperature-driving potential. Consequently, the rapid warming of the cooling medium diminishes the mean temperature difference between phases, further constraining heat-transfer performance.

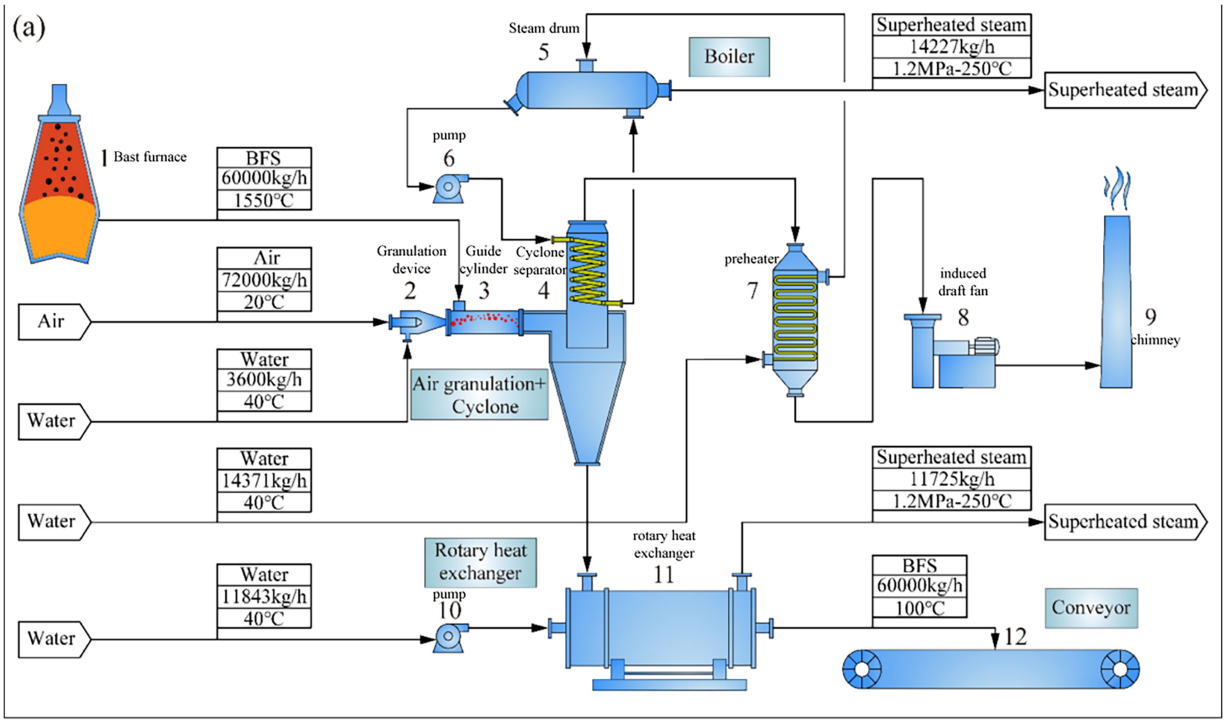

Figure 2: (Continued)

Figure 2: The blast-furnace slag waste-heat-recovery system. (**a**) The technology scheme for 60 t/h blast furnace slag disposal. (**b**) The industrial project. (**c**) The molten blast furnace slag. (**d**) The slag particles after treatment [43].

From a system-level perspective, Ma et al. [36] highlighted that optimized temperature control could enhance condensation-based heat recovery, achieving net energy gains of approximately 28.2 kWh. Similar conclusions were drawn by Rubio-López et al. [47], who demonstrated that coupling condensation and separation processes in a high-efficiency cyclonic system effectively improves both waste-heat utilization and particle removal performance.

(2) Dual effects of temperature on separation efficiency

Temperature exerts a twofold and sometimes opposing influence on particle separation. On one hand, higher gas temperature increases viscosity, which can reduce the effective centrifugal forces on particles and thereby lower separation efficiency [40]. Ma et al. [36] observed a decreasing trend in dust-removal performance as flue-gas temperature rose from 40°C to 70°C.

On the other hand, controlled cooling that triggers heterogeneous condensation can markedly improve capture of fine particles [41]. Ma et al. [36] further demonstrated that when hot flue gas (about 120°C) is cooled below the water dew point inside the cyclone, water vapor condenses on soot particles that act as condensation nuclei. The consequent growth in particle mass and size makes them easier to separate under centrifugal forces, boosting removal efficiency of submicron particles to around 91% [48]. This condensation-assisted pathway also recovers latent heat, creating a synergistic benefit: simultaneous enhancement of pollutant removal and energy recovery.

Elevated temperatures increase gas viscosity and decrease density, thereby intensifying particle drag and attenuating the centrifugal separation force [39,49]. Therefore, incorporating temperature-dependent property variations is essential for the optimal design of high-temperature cyclone separators [50].

(3) Synergistic optimization of separation and heat transfer for high-temperature applications

Based on the mechanisms, the integration of heat transfer efficiency and separation performance into unified optimization objectives has emerged as a pivotal trajectory in the advancement of high-temperature cyclone separators. Current research is shifting from passive analysis of thermal effects toward the proactive optimization of thermo-mechanical coupling processes. This transition signifies an evolution

in the research paradigm toward LCO framework, prioritizing the long-term operational sustainability and holistic efficiency of the system.

From one perspective, researchers are pursuing synergistic optimization through the development of integrated "separation-heat transfer" architectures. For instance, in the context of recovering converter gas at 850°C, recent studies have proposed the integration of evaporative heating surfaces directly into the walls of novel circulating fluidized cyclones to achieve simultaneous particulate abatement and sensible heat recovery. Numerical investigations have elucidated the internal flow field dynamics and heat flux distributions, revealing that the conical section contributes 40.2% of the total thermal exchange capacity. Such findings provide a critical foundation for the synergistic design of systems characterized by low ΔP, high-collection efficiency, and enhanced heat transfer [51]. This research trajectory demonstrates that internalizing waste heat recovery as a primary design constraint, coupled with multi-physics simulations, constitutes a robust technical pathway for achieving the dual imperatives of energy conservation and gas purification.

Conversely, significant strides have been made in embedding thermodynamic indicators directly into traditional separation performance optimization frameworks. In the optimization of cyclone preheaters for cement production, specific studies have defined both outlet gas temperature and η as competing objective functions. by leveraging an integrated approach that combines CFD with intelligent optimization algorithms, researchers have automated the refinement of geometric parameters. This methodology enables the identification of an optimal balance between separation and thermal recovery performance along the Pareto frontier [52]. Such advancements facilitate a transition of multi-physics considerations from post-hoc evaluation to the initial design phase, effectively realizing a leap from isolated hydrodynamic tuning to integrated, multi-disciplinary system synthesis.

2.2.2 Thermal Behavior of the Cyclone Separator in Cooling Use

The thermal behavior of cyclones when used for cooling or waste-heat recovery merits focused attention because the same temperature-driven processes that affect heat-transfer rates also feedback on flow structure and particle dynamics. The strong swirling flow that governs particle trajectories likewise enhances convective heat transfer, especially adjacent to the wall and within the conical section, so that local thermal gradients and residence-time differences directly influence both cooling effectiveness and separation outcomes. For high-temperature metakaolin particles, the presence of short-circuit flows and non-uniform residence times produces uneven gas–solid interaction and temperature deviations within the cyclone, reinforcing the coupling between hydrodynamics and thermal performance [51].

The gas-phase energy conservation equation can be expressed as:

$$\rho c_p \left(\frac{\partial T}{\partial t} + u \cdot \nabla T \right) = \nabla \cdot (k \nabla T) + S_{p-g}, \tag{5}$$

where S_{p-g} denotes the interphase heat source accounting for gas-solid exchange and possible latent heat effects.

Building upon this framework, Xu et al. [53] numerically analyzed gas-solid heat transfer in a kaolin cyclone cooling system using an Eulerian model with user-defined functions. Their results showed clear temperature stratification, with hot cores and cooler outer short-circuit regions, indicating strong thermal asymmetry linked to the spiral flow. As illustrated in Fig. 3, the twin cyclones (CC1 and CC2) exhibit distinct outlet temperatures and heat-transfer characteristics. As shown in Fig. 3b, due to the high air volume and short residence time in the heat exchanger tube, the cold air near the tube wall does not come into full contact with the hot metakaolin until there are still large areas of low temperature at the exit of the heat exchanger

tube. In combination with Fig. 3c, the high-temperature zone in the middle is the result of this part of the flow is in contact with the metakaolin particles for the longest time and receives the most heat.

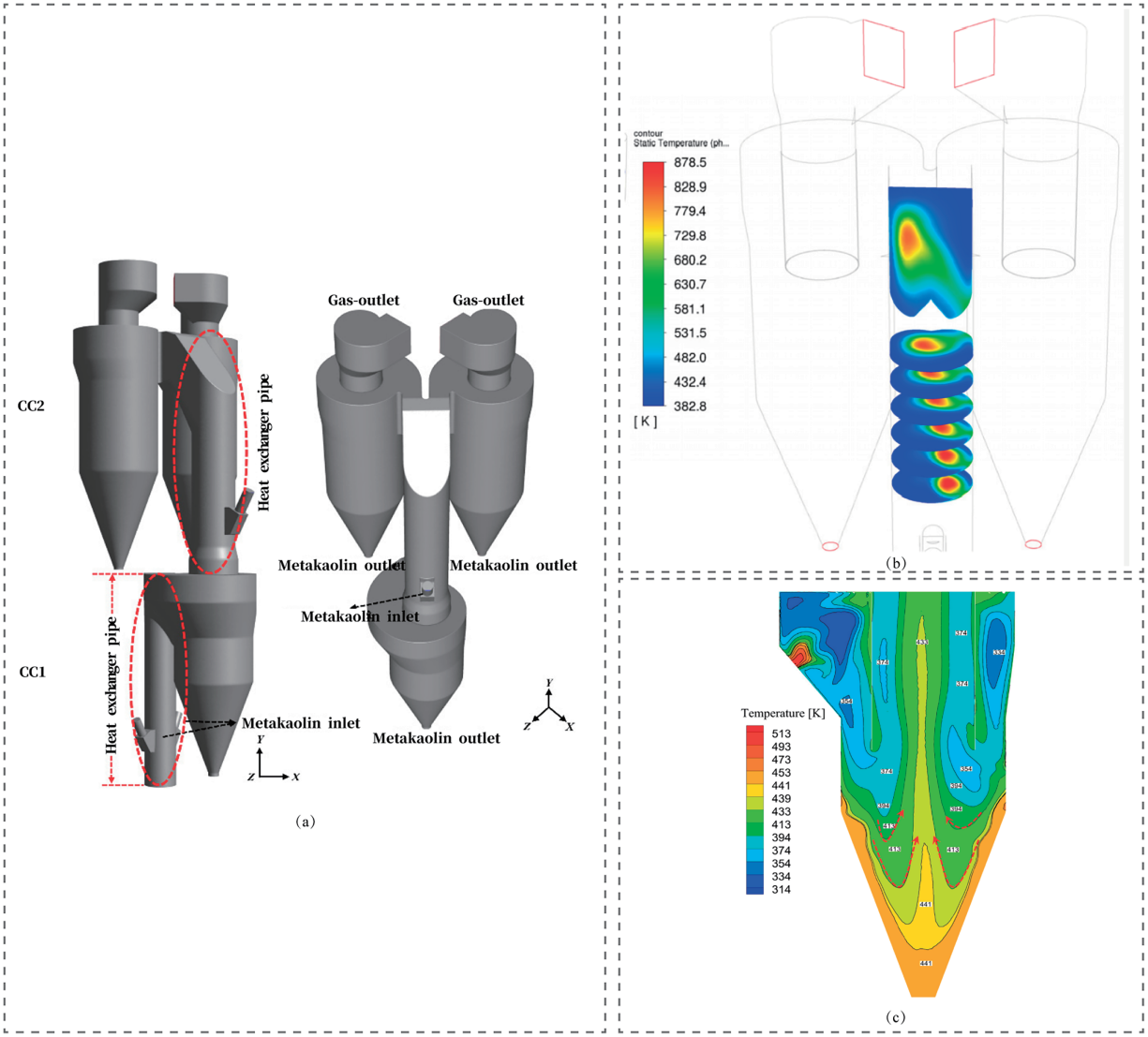

Figure 3: Legends for CC1 and CC2. (**a**) Cooling system model; (**b**) The temperature contour of CC2 cyclone; (**c**) Temperature contour of CC1 cyclone [53].

When the cyclone is operated with a wetted surface or as part of an evaporative cooling strategy, the wet-bulb effect and thermal efficiency should be considered. The cooling efficiency can be defined as [54]:

$$\eta_c = \frac{T_{in} - T_{out}}{T_{in} - T_{wb}}, \tag{6}$$

where, T_{in}, T_{out} and T_{wb} are the inlet, outlet and wet-bulb temperatures, respectively. Higher η implies better cooling performance but typically increases water consumption. In particle-laden flows, particle heat capacity and size distribution influence local temperature gradients and introduce thermal lag; such phenomena are best captured via coupled Eulerian–Eulerian or Eulerian-Lagrangian numerical frameworks.

Overall, temperature exerts a multifaceted influence on cyclone behavior by simultaneously altering the thermophysical properties of the gas-solid mixture, reshaping flow-driven heat transfer, and modifying particle separation characteristics through viscosity and condensation effects. These coupled mechanisms give rise to spatial temperature nonuniformities and dynamic feedback between heat and momentum transport. Consequently, the optimal design and operation of cyclones for cooling or waste-heat recovery should emphasize coordinated control of inlet temperature, cooling-medium parameters, and flow geometry to achieve a balanced improvement in both heat utilization and particulate removal efficiency.

2.3 Optimization Objectives and Approaches for Cyclone Separators

Optimization requires a comprehensive evaluation of relevant parameters to achieve an appropriate balance between separation efficiency and pressure drop, thereby ensuring that the equipment meets performance requirements across diverse application scenarios. Moreover, precise parameter selection can significantly reduce redundant computations and experimental efforts, lower overall costs, and improve the efficiency of the optimization process.

In different industries, it is crucial to prioritize optimization objectives based on specific operational requirements. Jiang et al. [27] achieved efficient separation of coarse particles by increasing the cylinder diameter ($D \geq 1.5$ m) and optimizing the aspect ratio ($H/D = 3–4$). This configuration utilized the combined effects of gravity sedimentation and centrifugal force to reduce the entrainment of fine particles, resulting in a dual improvement in both processing capacity and separation accuracy for a single device. In chemical catalyst recovery, where catalyst costs are high, the primary optimization target focuses on separation efficiency. Fatahian et al. [55] assigned a weight coefficient $\alpha 1$ to the separation efficiency ($\eta \geq 0.7$) while constraining ΔP to within 2000 Pa. This strategy improved recovery rates and minimized raw material losses while maintaining energy efficiency. For cyclone separators used in environmental dust removal, the key lies in balancing ΔP and η. Ma et al. [36] quantified ΔP using the Euler number (target value ≤ 80) and set the PM 2.5 η as a strict constraint. They further optimized the axial inlet and guide vanes to achieve a balance between efficiency and energy consumption, ensuring compliance with the $PM \leq 10$ mg/m^3 emission standard.

In the pharmaceutical and food industries, both cleanliness and η are of equal importance. Soliman et al. [56] developed a nonlinear optimization model that incorporates surface characteristics, treating surface roughness ($Ra \leq 0.8$ μm) and particle retention rate ($R \leq 0.1\%$) as penalty terms ($\beta_1, \beta_2 \geq 1000$). By controlling the exhaust pipe insertion depth ($h/D = 0.3–0.5$) and employing an electrolytic polishing process, they achieved a particle η of ≥99% while ensuring compliance with GMP standards. In optimization of circulating fluidized bed boilers, the primary focus is on wear rate reduction. Wang et al. [57] assigned a high wear weight coefficient $\gamma \geq 500$ and, by limiting the cone wall impact velocity and utilizing a ZGMn13 cast steel lining with a thickness of $\delta \geq 5$ mm, they maintained the wear rate below 0.1 mm/kh. This design ensured an equipment lifespan exceeding 8000 h and reduced the loss from incomplete combustion of solids to below 3%. These studies collectively contributed to the establishment of a comprehensive three-dimensional optimization framework emphasizing the integration of efficiency, durability, and energy consumption.

The design of cyclone separators requires the establishment of optimization goals tailored to industry-specific working conditions. Different objective function systems are formulated, influenced by factors such as process constraints, economic efficiency, and industry standards and specifications under varying operating conditions.

3 Evolution of Cyclone Separator Optimization Design

The optimization design of cyclone separators has evolved from empirical trial-and-error to a precision paradigm integrating experimental research, theoretical modelling, and numerical simulation. While CFD

provides detailed characterization of internal flow fields, its high computational cost in multi-parameter collaborative optimization remains a significant bottleneck. To address this, current research increasingly adopts a collaborative strategy integrating CFD with surrogate models and intelligent algorithms. This approach enables the efficient exploration of high-dimensional parameter spaces, significantly enhancing both design reliability and efficiency.

3.1 Numerical Framework and Validation

3.1.1 Turbulence Models and Governing Equations

The internal flow within a cyclone separator is characterized by strong swirling motion, highly anisotropic turbulence, and complex two-phase interactions that are difficult to capture using conventional experimental techniques. CFD, when combined with refined physical and numerical models, can depict fine-scale flow phenomena inside cyclone separators, including coherent vortex structures and detailed particle trajectories [58].

(1) Turbulence models

To resolve the detailed distributions of tangential velocity, axial velocity, and static pressure, CFD is widely applied. Models based on the Reynolds-averaged Navier-Stokes (RANS) equations remain the most used approach for predicting time-averaged flow characteristics because of their favorable balance between accuracy and computational cost. Within the RANS framework, turbulence closure is achieved through various modeling strategies. Owing to the high shear rates and pronounced turbulence anisotropy inside cyclone separators, the Reynolds stress model generally provides more reliable predictions than standard eddy-viscosity models such as $k-\varepsilon$ or $k-\omega$ [59]. For instance, Sun et al. [60] simulated an axial cyclone separator using the Reynolds stress model and revealed that geometric parameters such as blade angle and exhaust pipe insertion depth significantly influence the internal flow structure.

For investigations that aim to resolve unsteady flow behavior and transient vortex structures, large eddy simulation (LES) is widely employed [61]. LES offers higher temporal and spatial resolution by directly resolving the large-scale turbulent eddies while modeling the dissipation of small-scale motions through a sub-grid scale model. Although LES provides a more detailed representation of the flow field, it typically demands substantially greater computational resources compared with RANS-based approaches [62].

(2) Governing equations

The core foundation of CFD rests upon the governing equations of fluid flow, which mathematically describe the fundamental principles of physics. These equations primarily consist of three conservation laws: mass conservation equation (continuity equation), momentum conservation equation (Navier-Stokes equations) and energy conservation equation.

All flow problems must satisfy the fundamental law of conservation of mass. This law states that the increase in mass of a fluid element per unit time is equal to the net mass flowing into the element over that time interval. According to this principle, the mass conservation equation, also known as the continuity equation, can be derived [63]:

$$\frac{\partial \rho}{\partial t} + \nabla \cdot (\rho V) = 0 \tag{7}$$

where V represents velocity vector, t represents time, ρ represents density.

The momentum conservation equation is a fundamental law that must be satisfied by any fluid flow system. This law is essentially the application of Newton's second law to a fluid element. It states that the rate

of change of momentum of a fluid in an infinitesimal element with respect to time is equal to the net sum of all forces acting on that element. According to this law, the momentum conservation equations, commonly known as the Navier-Stokes equations, can be derived for the x, y, and z directions [63]:

x component:

$$\frac{\partial(\rho u)}{\partial t} + \nabla \cdot (\rho u V) = -\frac{\partial p}{\partial x} + \frac{\partial \tau_{xx}}{\partial x} + \frac{\partial \tau_{yx}}{\partial y} + \frac{\partial \tau_{zx}}{\partial z} + \rho f_x \tag{8}$$

y component:

$$\frac{\partial(\rho v)}{\partial t} + \nabla \cdot (\rho v V) = -\frac{\partial p}{\partial y} + \frac{\partial \tau_{xy}}{\partial x} + \frac{\partial \tau_{yy}}{\partial y} + \frac{\partial \tau_{zy}}{\partial z} + \rho f_y \tag{9}$$

z component:

$$\frac{\partial(\rho w)}{\partial t} + \nabla \cdot (\rho w V) = -\frac{\partial p}{\partial z} + \frac{\partial \tau_{xz}}{\partial x} + \frac{\partial \tau_{yz}}{\partial y} + \frac{\partial \tau_{zz}}{\partial z} + \rho f_z \tag{10}$$

where τ_{ij} is the viscous stress tensor representing the force due to fluid viscosity, p represents the static pressure, u, v, w represent the velocity components in the x, y, z directions and f represents the body force per unit volume or mass.

The law of conservation of energy is one of the fundamental laws that must be satisfied by fluid systems involving heat exchange. This law is essentially the mathematical expression of the first law of thermodynamics applied to a continuous medium. The total energy of a fluid is typically the sum of three components: internal energy, kinetic energy $K = 1/2(u^2 + v^2 + w^2)$, and potential energy. In practical engineering applications, particularly for low-speed flows where kinetic and potential energy changes are negligible, the conservation equation can be simplified to focus on the internal energy or enthalpy. Given the thermodynamic relationship: e = c_vT (where c_v is the specific heat capacity at constant volume), the conservation equation can be derived with temperature as the main variable [63,64]:

$$\frac{\partial(\rho c_v T)}{\partial t} + \nabla \cdot (\rho c_v T V) = -p(\nabla \cdot V) + \Phi + \nabla \cdot (k \nabla T) \tag{11}$$

where c_v represents the specific heat capacity at constant volume, T represents temperature, k represents the thermal conductivity of the fluid, Φ represents the viscous dissipation function.

3.1.2 Euler-Lagrange Particle Tracking Approaches

In gas-solid two-phase flow systems, accurate tracking of particle motion and evaluation of separation efficiency are essential. DPM, formulated within the Euler–Lagrange framework, is widely adopted to resolve individual particle trajectories and to quantify size-dependent separation performance [65]. In this approach, the continuous gas phase is obtained by solving the Eulerian governing equations, while the dispersed particles are tracked by integrating the Lagrangian equations of motion. The particle momentum equation typically accounts for drag force, lift force, virtual mass force, and Brownian motion [66], and can be written as [67]:

$$m_p \frac{du_p}{dt} = \sum F_i, \tag{12}$$

where m_p is the particle mass, u_p denotes the particle velocity vector, and $\sum F_i$ represents the resultant force acting on the particle.

Within the DPM framework, researchers can quantify particle residence time and elucidate the mechanisms that govern particle trapping. For example, Gopalakrishnan et al. [68] demonstrated that blade length substantially alters residence time and has a pronounced effect on separation efficiency. Accurate representation of particle–particle interactions and of particle–wall rebound behavior is also essential when simulating high solids loadings and when aiming to predict realistic separation performance [69].

3.1.3 Grid Independence and Validation Strategies

Although CFD provides a cost-effective, readily parameterizable alternative to resource-intensive experiments, rigorous verification of numerical results remains essential [70]. Ensuring numerical accuracy begins with a grid-independence study: simulations are carried out on a series of progressively refined meshes to assess whether key flow-field quantities (e.g., velocity, pressure, separation efficiency) change meaningfully with further refinement. Once these quantities have converged, discretization error can be considered negligible and the numerical predictions regarded as reliable [71].

Model calibration and validation require high-quality experimental measurements. Common techniques include particle image velocimetry and laser doppler velocimetry for resolving the flow-field velocity, while η validation is typically performed by comparing particle size distributions measured at the inlet and outlet [72]. Once the numerical model has been rigorously validated against experimental data, it can be used *in silico* for systematic parameter studies and multi-scenario simulations, substantially accelerating the design-optimization process.

3.2 Intelligent Optimization Strategy

Directly coupling CFD with optimization algorithms is often impractical due to the time-intensive nature of high-fidelity simulations [73]. The introduction of surrogate models as an intermediate layer effectively mitigates this computational burden [74].

Surrogate models (Table 1), such as response surface methodology (RSM), radial basis function (RBF) networks, and Kriging function as mathematical approximations of the computationally expensive CFD solver [75]. These models establish a rapid mapping relationship between design parameters and performance indicators based on a limited set of high-fidelity sample points. For example, Babaoğlu et al. utilized a radial basis function neural network (RBFNN) trained on 42 Latin hypercube sampled datasets, which maintained prediction errors below 5% while drastically reducing the required number of full CFD simulations.

Table 1: Comparison of common surrogate models.

Model	Modeling Prerequisites	Scope of Application	References
RSM	DOE must fully cover the design space to minimize interpolation error; polynomial order requires a trade-off, too low causes underfitting and misses nonlinearities; too high induces overfitting.	Well-suited for engineering modeling and optimization with limited samples (tens-hundreds); typical applications: polynomial response-surface approximation; coarse-grained CFD surrogate modeling; global sensitivity analysis; rapid parameter-space screening.	[76,77]

(Continued)

Table 1 (continued)

Model	Modeling Prerequisites	Scope of Application	References
RBF	Computational cost scales as O (n^3), imposing a heavy burden for large datasets; predictive accuracy is highly sensitive to basis-function and shape-parameter choices, requiring rigorous hyperparameter tuning.	Well-suited for interpolation and fitting with limited samples, medium dimensionality, and sharp local features or discontinuities; applications include high-precision interpolation of complex flow structures, stress concentrations; precise fine-fitting of response surfaces with spikes or fault signatures.	[78,79]
Support vector regression (SVR)	SVR predictive performance is highly sensitive to hyperparameters-penalty (C), insensitive-loss (ε), and kernel parameters; improper tuning yields underfitting or overfitting.	Well-suited for nonlinear regression with small-moderate sample sizes (tens-thousands); typical applications: sensor calibration; short-term forecasting; remote-sensing spectral inversion; constitutive-model fitting for small-sample material datasets.	[80,81]
Kriging	Predictive fidelity depends on careful selection and estimation of the correlation function and its hyperparameters, which often incurs significant computational overhead; Kriging yields both mean predictions and an explicit prediction-uncertainty metric.	Ideally suited for computationally expensive function approximation and optimization; applicable to sample sizes from tens to thousands; high-value applications: CFD-based parametric optimization; Bayesian optimization with acquisition functions; environmental spatial interpolation and mapping from sparse observations; efficient stepwise experimental design.	[82,83]

However, the efficacy of surrogate models is subject to several critical limitations. In high-dimensional design spaces, the complexity of the surrogate model increases exponentially [84]. This often leads to a phenomenon where the model overfits the limited training data, effectively fitting noise rather than the underlying physical trend. Models like RSM, which rely on low-order polynomials, may fail to capture the high nonlinearity of fluid dynamics in complex geometries, while more flexible models like RBFNN risk overfitting if the training dataset is sparse.

The reliability of a surrogate model is fundamentally dependent on the quality and quantity of its input data [85]. Generating enough high-fidelity CFD data points for training remains a time-consuming and expensive process, which itself forms the initial bottleneck that surrogate modeling is intended to solve. Inadequate data density can lead to large interpolation errors.

Surrogate models are optimized for interpolation within the sampled design domain [86]. Their predictive capability degrades significantly when required to extrapolate outside this defined space. Since optimization algorithms often search for extremes at the boundaries of the design space, this inherent extrapolation uncertainty can lead the optimization process toward physically unreliable optimal solutions.

Driven by the surrogate model, intelligent algorithms (Table 2) perform systematic searches within the design space. Algorithms such as genetic algorithms (GA), particle swarm optimization (PSO), and non-dominated sorting genetic algorithm II (NSGA-II) emulate natural selection or swarm behavior to handle nonlinear, multi-peak problems. This integration allows for the evaluation of thousands of design iterations in seconds, a scale unachievable with direct CFD coupling, provided the underlying surrogate model is accurate.

Table 2: Common optimization algorithms.

Optimization Algorithm	Advantages	Disadvantages	Scope of Application	References
GA	Exhibits strong global search ability and is effective for nonlinear structural optimization.	Low computational efficiency and high structural optimization cost.	Applicable to topology, shape, size, and multi-objective comprehensive optimization.	[87,88]
NSGA-II	Combines the global search capability of genetic algorithms with flexible constraint handling strategies.	High computational complexity limits the efficiency of large-scale optimization.	Applicable to multi-objective structural optimization in fields such as aerospace and mechanical engineering.	[89,90]
PSO	Interaction between individual and group information enables efficient global search.	Prone to falling into local optima in complex multi-peak structure optimization.	Applicable to structural optimization problems with continuous objective functions.	[91–93]
Differential evolution algorithm	Utilizes differential mutation and crossover operations, offering significant advantages in continuous variable optimization.	Prone to falling into local optima in complex multi-peak structure optimization.	Applicable to structural optimization problems dominated by continuous variables.	[94–96]
Non-dominated sorting genetic algorithm III (NSGA-III)	Maintains diversity among individuals in the population by providing and adaptively updating a set of well-distributed reference points.	Performance is sensitive to the distribution and number of references points, and require more parameter tuning.	Specifically designed for multi-objective optimization problems (M > 3 objectives), especially relevant in complex engineering design.	[97,98]

3.3 Integrating CFD with Computational Intelligence in Cyclone Optimization

The collaborative optimization framework typically follows a closed-loop process: definition of objectives, key parameter screening, CFD data generation, surrogate model training, and algorithmic optimization (Fig. 4).

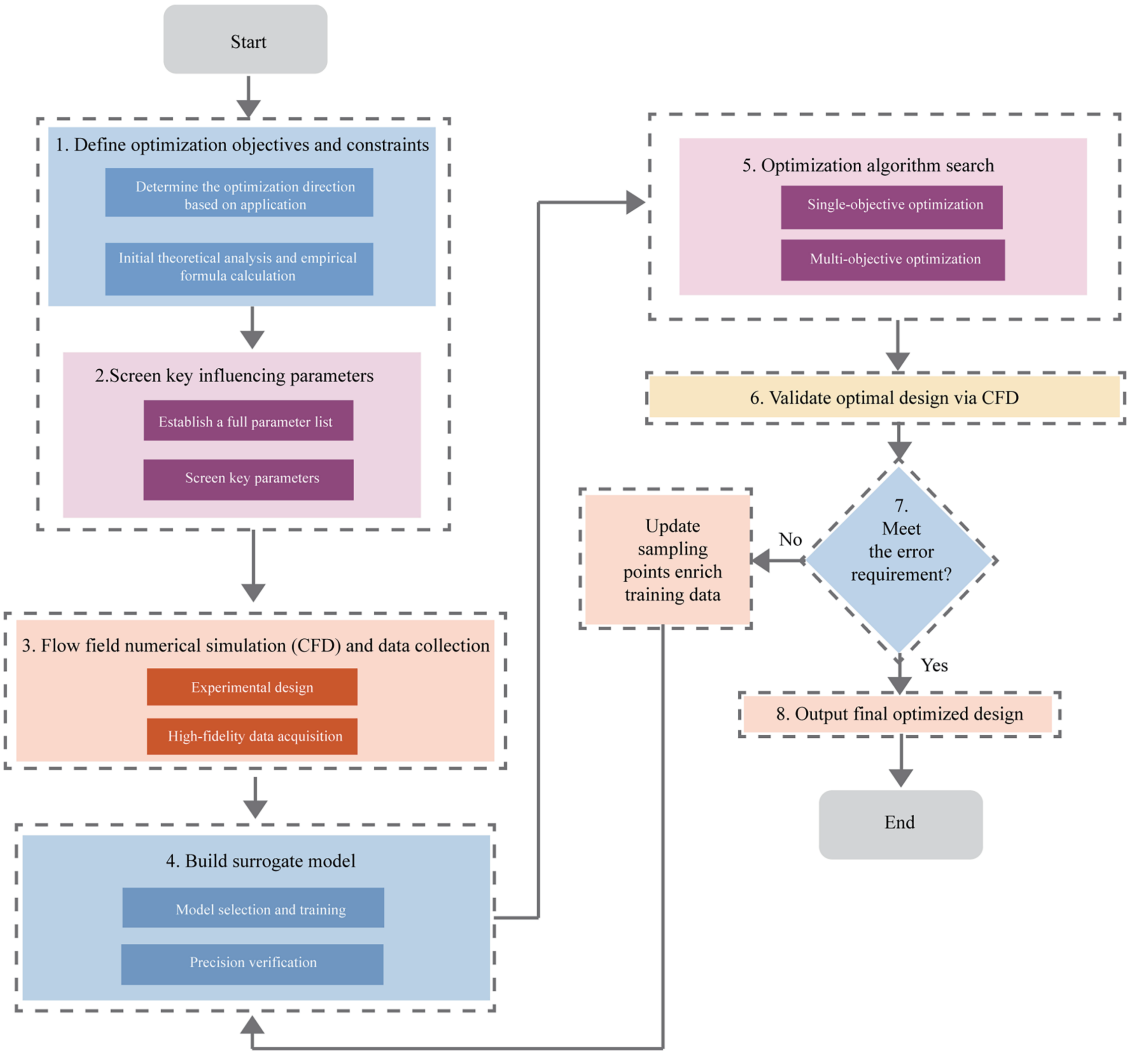

Figure 4: Optimization process of the cyclone separator.

3.3.1 Single-Objective Optimization Examples

Single-objective optimization targets specific metrics, such as η or ΔP, to meet defined operational requirements [27,32].

Li et al. [99] focused on enhancing the removal of 8 μm particles for high-precision applications. By constructing a second-order response surface model based on four geometric parameters (including guide vane angle and exhaust diameter), the study achieved a twofold increase in η, though this was accompanied by a 69.32% rise in ΔP.

Conversely, Ning et al. [100] targeted pressure drop reduction for energy-constrained systems. Through response surface optimization of eight geometric factors, ΔP was reduced by 69.8%, significantly improving operational economy.

While effective for specific targets, single-objective approaches often fail to balance conflicting requirements, such as the inherent trade-off between η and energy consumption.

3.3.2 Multi-Objective Collaborative Optimization

Multi-objective optimization addresses these conflicts by constructing a Pareto frontier, offering a set of non-dominated solutions that balance competing goals [57,101].

Sun and Yoon [102] combined a central composite design-based response surface model with the NSGA-II algorithm. The optimized design reduced ΔP by 7.38% and increased η by 3.11% relative to the reference model and outperformed the classic stairmand design with a 19.23% ΔP reduction.

Deng et al. [103] developed a framework integrating CFD, support vector machines, and NSGA-II to optimize guide vane geometry. The study quantified the non-linear trade-offs, describing η-ΔP relationship via a derived power-law function.

Elsayed [104] employed co-Kriging models with genetic algorithms, reducing ΔP to 22% of the Stairmand model baseline. Similarly, Pandey et al. utilized LES data to drive multi-objective optimization, achieving simultaneous improvements in ΔP (−43.22%) and η (+24.69%).

Table 3 summarizes various optimization strategies to better demonstrate the application of multi-objective optimization in cyclone separators.

Table 3: Comparative summary of optimization algorithms, objective functions and results for cyclone separators.

Optimization Strategy	Objective Functions	Results	References
ANNS; NSGA-II; (Latin hypercube sampling)	ΔP; η	ΔP decreased by 47.45%; η decreased by 3.62%	[90]
LHS; NSGA-II	ΔP; η	ΔP decreased by 11%; η increased by 4.2%	[105]
RSM; NSGA-II	ΔP; η	ΔP decreased by 2.7%; η increased by 1.01%	[106]
RSM; NSGA-II	ΔP; η	Design 1 ΔP increased by 69.0%; η increased by 20.88% Design 2 ΔP increased by 12.2%; η decreased by 15.76% Design 3 ΔP decreased by 23.6%; η increased by 3.76%	[68]
Group method of data handling-type neural networks; PSO	ΔP; η	ΔP increased by 62.2%; η increased by 96.5%	[107]
RBFNN; MOPSO	Eu; Stk_{50};Stk_{100}	Design 1 Eu increased by 14%; Stk_{50} decreased by 37%; Stk_{100} decreased by 40% Design 2 Eu increased by 23%; Stk_{50} decreased by 20%; Stk_{100} decreased by 48% Design 3 Eu increased by 79%; Stk_{50} decreased by 49%; Stk_{100} decreased by 73% Design 4 Eu increased by 360%; Stk_{50} decreased by 57%; Stk_{100} decreased by 84%	[108]

(Continued)

Table 3 (continued)

Optimization Strategy	Objective Functions	Results	References
SVR; MOPSO	Eu; Stk_{50}	Design 1 Eu decreased by 96.34%; Stk_{50} increased by 35.4% Design 2 Eu increased by 415.7%; Stk_{50} increased by 83.64%	[109]
10 meta-heuristic algorithms	ΔP; η	Design 1 ΔP decreased by 3.3%; η increased by 6.0% Design 2 ΔP decreased by 27.5%; η increased by 0.36% Design 3 ΔP decreased by 14.4%; η increased by 3.5%	[110]
Multi-objective surrogate-based optimization	ΔP; η	ΔP decreased by 9.1%; η decreased by 33.1%	[111]
RSM; Desirability function approach	ΔP; η; Stk_{50}	ΔP decreased by 20.70%; η increased by 24.22%; Stk_{50} decreased by 75.38%	[112]

Despite these advancements, the field faces challenges regarding the high computational cost of generating high-fidelity training data and the potential for surrogate model bias in highly nonlinear regions. Furthermore, theoretical Pareto solutions may occasionally exceed manufacturing constraints. Future research should focus on adaptive sampling strategies to improve model efficiency and the incorporation of full-lifecycle costs into the optimization objective function.

4 Examples and Applications of Cyclone Separator Optimization

The optimization of cyclone separators aims to address engineering challenges through innovative approaches. The previously described framework, which integrates CFD simulation, surrogate models, and intelligent optimization algorithms, provides a critical technical pathway for this purpose. The effectiveness of this pathway must be validated through specific case studies [113]. This section analyzes the key issues addressed and the application outcomes of optimized cyclone separators in representative industrial fields, evaluating their operational performance using typical examples and data. The objective is to guide the rational selection and performance enhancement of cyclone separators across a broader range of industrial applications.

The complex nonlinear relationships between geometry, operating conditions, and performance render exclusive reliance on high-fidelity simulations computationally prohibitive for design exploration. To address this limitation, hybrid data-driven approaches have proven effective. For instance, Zhang et al. [93] utilized a dataset comprising 217 experimental cases, employing PCA for feature reduction and SVR model tuned via PSO. This methodology achieved highly accurate performance prediction (R^2 = 0.982), thereby demonstrating the feasibility of efficient modeling using limited data.

A pervasive challenge is balancing the inherent trade-off between ΔP and η, a classic multi-objective optimization problem. Several studies have successfully addressed this using surrogate model-based optimization. Sun and Yoon [102] and Elsayed and Lacor [114] built surrogates from high fidelity CFD data, specifically RSM and RBFNN. They coupled with GA to obtain Pareto fronts that provide a range of design options balancing ΔP and η without exhaustive simulations. To improve robustness and efficiency in complex design spaces, Singh et al. [111] proposed an efficient multi-objective (EMO) algorithm, which uses an ensemble of surrogate models including Kriging, RBF and SVR together with adaptive model selection. This approach reduced required CFD evaluations from thousands to about 150 while effectively exploring trade-offs between Eu and Stk_{50}.

This framework also applies when cyclone separation principles are extended to other processes, such as waste heat recovery using vortex generator enhanced heat exchangers. Hatami et al. [115] combined experimental data (the experimental setup is shown in Fig. 5a) and CFD data to perform an exergy analysis and used RSM to quantify how operating parameters affect recovered exergy and irreversibility. Their optimization identified operating conditions that maximize exergy recovery while minimizing losses. As shown in Fig. 5b,c, the RSM response surfaces clearly illustrate parameter dependencies and the locations of optimal operating points. The vortex generator configuration increases heat transfer without producing excessive back pressure that would impair engine performance. These findings demonstrate the method's versatility for optimizing both thermodynamic performance and gas solid separation.

While individual cases target different objectives, they are unified by the integrated framework of high-fidelity data, surrogate modeling and intelligent optimization proposed in this study. Their successful implementation validates the framework's robustness and effectiveness. All applications rely on high-fidelity datasets: studies [102,111,114] use CFD simulations and studies [93,115] use experimental measurements. To reduce the computational burden of physical modeling, efficient surrogate architectures were developed, including SVR [93], RSM [102,115], RBFNN [114], and model ensembles [111]. These surrogates were then paired with intelligent optimization algorithms such as PSO [93], GA [102,114], EMO [111], and RSM-based numerical techniques [115]. This multi-level workflow enables automated identification of optimal design configurations and demonstrates a general methodological pathway for addressing complex optimization challenges in cyclone separator design.

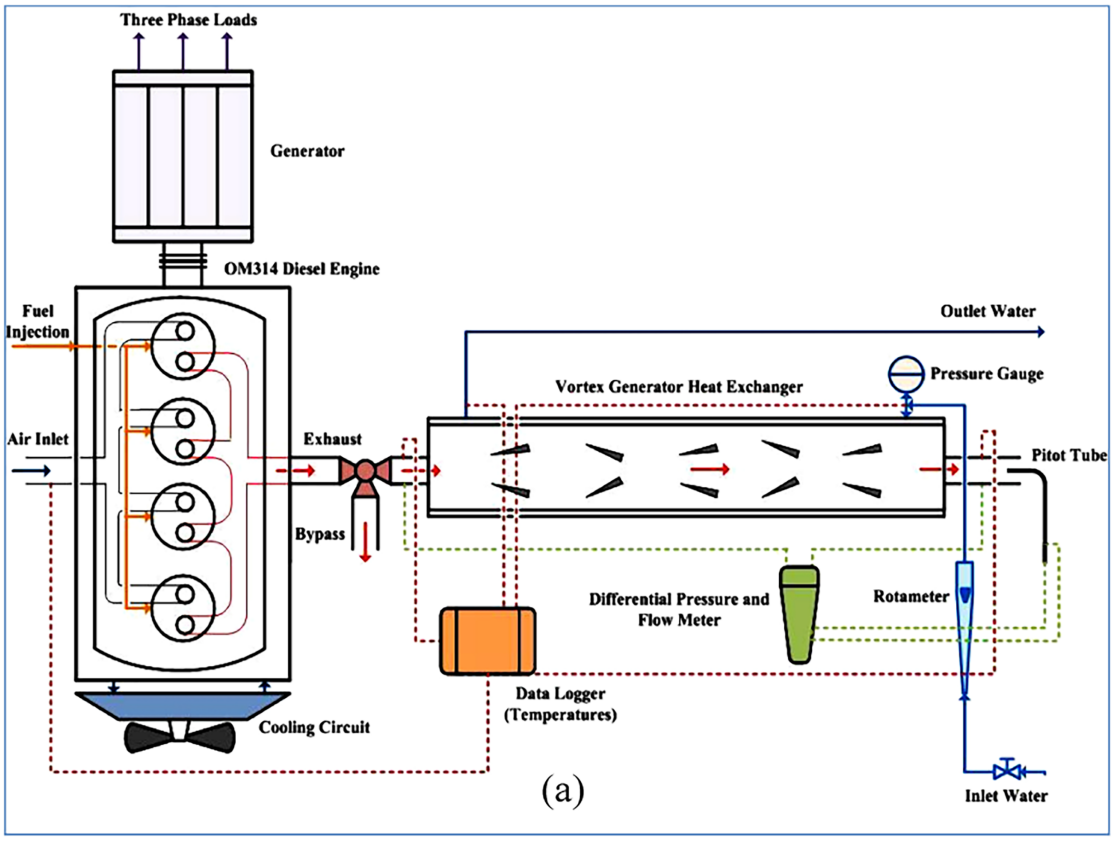

Figure 5: (Continued)

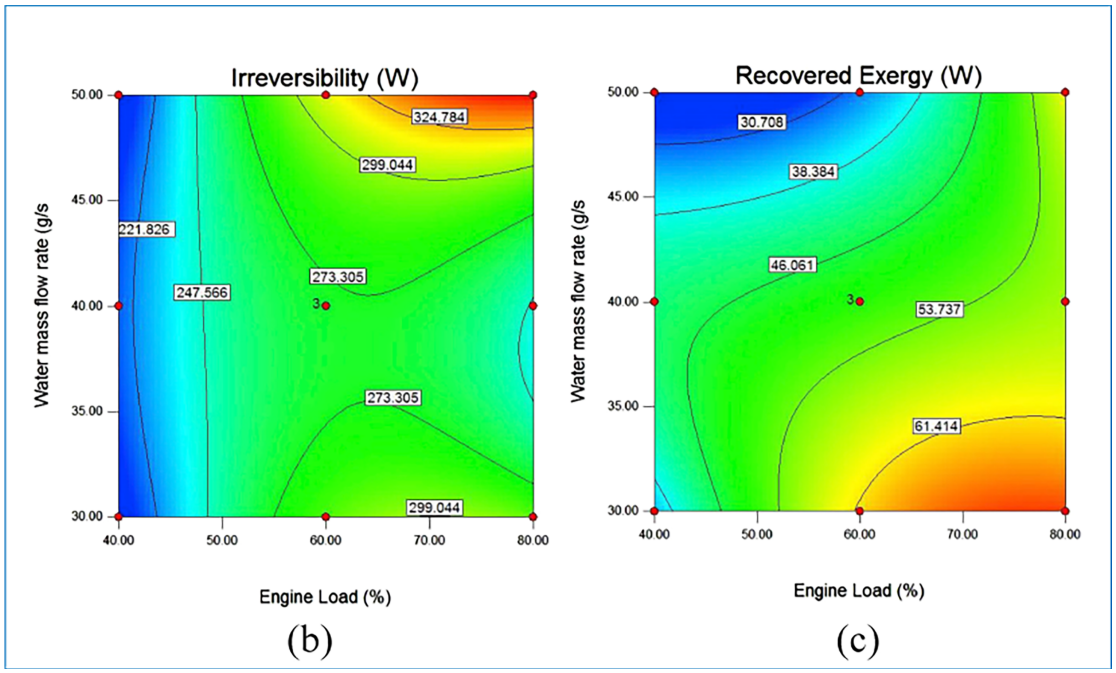

Figure 5: Exergy performance optimization of vortex generator heat exchanger. (**a**) Schematic of experimental setup. (**b**) Contour of effect of engine load and water mass flow rate on irreversibility. (**c**) Contour of effect of engine load and water mass flow rate on recovered exergy [115].

5 Conclusions and Outlook

Through a systematic review of the optimal design of cyclone separators, this study confirms that a relatively mature theoretical and technical framework has been established in the field. At the theoretical level, research has clarified the fundamental role of dimensionless parameters (Stk, Re_p) in governing separation performance and flow stability, guiding the optimization of key structural parameters (i.e., cylinder/cone lengths). Theoretical analyses have also recognized that temperature and heat-transfer behavior constitute an essential part of the theoretical foundation, as thermal variations simultaneously modify gas–solid properties, flow organization, and energy-transfer mechanisms within the cyclone. Methodologically, the field has undergone a critical paradigm shift from empirical trials to simulation-driven workflows. CFD serves as the core tool for flow mechanism elucidation, while surrogate models significantly reduce the computational cost of high-fidelity simulations. Crucially, the integrated framework of CFD, surrogate models, and multi-objective evolutionary algorithms (e.g., NSGA-II) has emerged as the standard approach for successfully escalating design objectives to customized, multi-objective optimization tailored for diverse industrial demands.

Despite these advances, the effective industrial deployment and long-term value of optimization outcomes are fundamentally limited by the follow critical gaps: (1) Multi-objective Pareto solutions often lack robustness under dynamic operating conditions and may violate manufacturing tolerances. (2) Recent studies incorporate thermal stress, separation efficiency and waste-heat recovery into optimization models, forming the basis of LCO framework. A complete LCO must extend to long-term system-level optimization that dynamically couples physical performance, lifecycle energy use and economic metrics such as operating costs and depreciation. Existing models and empirical studies remain nascent, hindering the shift from equipment-level design to system-value optimization. (3) In complex, high-dimensional design spaces,

surrogate model accuracy is highly sensitive to sample distribution, frequently necessitating costly repeated CFD validation to ensure reliability.

To overcome these challenges, future research should progress in three key directions: (1) Expand the optimization framework to multi-physics coupling, integrating CFD–DPM simulations with models of material wear, structural stress, and conjugate heat transfer, including phase-change and heat-recovery effects, to jointly evaluate separation and thermal performance. (2) Establish an LCO framework that incorporates thermal performance and waste-heat recovery economics (e.g., recovered energy, latent heat, and net present value) to optimize long-term operational benefits rather than short-term efficiency. (3) Develop intelligent decision systems based on digital twin technology that integrate real-time temperature and humidity data with adaptive surrogate models to ensure robust separation and heat-recovery performance under dynamic operating conditions.

Acknowledgement: This work was supported by the Qilu University of Technology (Shandong Academy of Sciences), Jinan, China; the Major Innovation Project of Qilu University of Technology (Shandong Academy of Sciences) (No. 2025ZDZX03); and the Science and Technology Small and Medium-Sized Enterprise Innovation Capacity Enhancement Project of Shandong Province (No. 2024TSGC1006).

Funding Statement: This work was supported by the Qilu University of Technology (Shandong Academy of Sciences) in Jinan, China. The authors have no financial or personal relationships to disclose that could be perceived as biasing their work.

Author Contributions: The authors confirm contribution to the paper as follows: study conception and design: Liying Gao, Bin Li; data collection: Bin Li; analysis and interpretation of results: Bin Li, Liying Gao; draft manuscript preparation: Bin Li, Liying Gao, Yong Li, Kun Zhu, Zhenling Fu, Shifan Xu, Mohan Li. All authors reviewed and approved the final version of the manuscript.

Availability of Data and Materials: Not applicable.

Ethics Approval: Not applicable.

Conflicts of Interest: The authors declare no conflicts of interest.

Nomenclature

D	Cyclone diameter
D_x	Exhaust pipe diameter
a	Inlet height
b	Inlet width
H	Total separator length
S	Exhaust pipe insertion depth
B_c	Cone bottom diameter
h	Cylindrical height
θ	Cone angle
L_i	Inlet length
d_{crit}	Critical escape particle size
d_p	Particle diameter
ρ	Air density
ρ_p	Particle density
v_i	Air inlet velocity
u_{in}	Inlet velocity

T	Temperature
T_{in}	Inlet temperature
T_{out}	Outlet temperature
T_{wb}	Wet-bulb temperature
R_a	Surface roughness
R	Particle retention rate
Stk	Stokes number
Eu	Euler number
η	Separation efficiency
η_c	Cooling efficiency
ΔP	Pressure drop
R^2	Correlation coefficient
Re	Reynolds number
Rep	Particle Reynolds number
ε	Residual
β	Penalty term
C	Penalty factor
C_i	Inlet particle concentration
C_D	Particle drag coefficient
μ	Fluid viscosity
γ	Wear weighting coefficient
δ	Thickness
τ_p	Particle relaxation time
τ_f	Characteristic time of the fluid
CFD	Computational fluid dynamics
LCO	Lifecycle optimization
DPM	Discrete phase model
PCA	Principal component analysis
ANNS	Artificial neural networks
LHS	Latin hypercube sampling
RANS	Reynolds-averaged Navier-Stokes
LES	Large eddy simulation
RSM	Response surface methodology
RBF	Radial basis function
RBFNN	Radial basis function neural network
SVR	Support vector regression
GA	Genetic algorithms
PSO	Particle swarm optimization
NSGA-II	Non-dominated sorting genetic algorithm II
NSGA-III	Non-dominated sorting genetic algorithm III
EMO	Efficient muti-objective

References

1. Wang H, Lu CX. Structural optimization and operational performance analysis of cyclone separators in a 3.6Mt/a catalytic cracking unit. Chem Ind Eng Prog. 2025;44(6):3238–46. (In Chinese). doi:10.16085/j.issn.1000-6613.2024-1802.
2. Gao Z, Wang J, Wang J, Mao Y. Time-frequency analysis of the *Vortex* motion in a cylindrical cyclone separator. Chem Eng J. 2019;373(3):1120–31. doi:10.1016/j.cej.2019.05.054.

3. Zhang YL, Liu PK, Zhang YK, Yang XH, Jiang LY. Experimental study on fly ash classification of hydrocyclone. China Powder Sci Technol. 2017;23(4):77–81. (In Chinese). doi:10.13732/j.issn.1008-5548.2017.04.016.
4. Zhang JY, Sun Q, Wang P. Study on the dust removal performance of a columnar cyclone separator. Contemp Chem Res, 2025(3):52–4. doi:10.20087/j.cnki.1672-8114.2025.03.017.
5. Reinking Z, Whitty KJ, Lighty JS. Design of a gas-solid-solid separator to remove ash from circulating fluidized bed reactors. Powder Technol. 2022;404:117467. doi:10.1016/j.powtec.2022.117467.
6. Shi D, Huang Y, Wang H, Yuan W, Fu P. Deoiling of oil-coated catalyst using high-speed suspending self-rotation in cyclone. Sep Purif Technol. 2019;210(1):117–24. doi:10.1016/j.seppur.2018.03.059.
7. Zhang P, Ji L, Han T, Li Y, Qi L. Multi-field coupling and synergistic removal of fine particles in coal-fired flue gas. Fuel. 2019;255(7):115746. doi:10.1016/j.fuel.2019.115746.
8. Xu Y, Chen G, Qin YQ, Li P, Zhou DD, Zhang JX. Study on the influence of dust discharge structure on the separation characteristics of a cyclone separator. Guangdong Chem Ind. 2025;52(16):79–82. (In Chinese). doi:10.3969/j.issn.1007-1865.2025.016.023.
9. Dimitrijević D, Schmid M, Harasek M, Bösenhofer M. Comparison of experimental, empirical, and CFD pressure losses of lab-scale sampling cyclones. Sep Purif Technol. 2025;354(2):128992. doi:10.1016/j.seppur.2024.128992.
10. Mazyan WI, Ahmadi A, Brinkerhoff J, Ahmed H, Hoorfar M. Enhancement of cyclone solid particle separation performance based on geometrical modification: numerical analysis. Sep Purif Technol. 2018;191(1135):276–85. doi:10.1016/j.seppur.2017.09.040.
11. Misiulia D, Elsayed K, Andersson AG. Geometry optimization of a deswirler for cyclone separator in terms of pressure drop using CFD and artificial neural network. Sep Purif Technol. 2017;185(3):10–23. doi:10.1016/j.seppur.2017.05.025.
12. Dong LL, Zhao YP, Liang LQ, Zhu Y, Duan GH. Review on theory and approach of mechanical optimization design. Mach Tool Hydraul. 2010;38(15):114–9. (In Chinese). doi:10.3969/j.issn.1001-3881.2010.15.036.
13. Shastri R, Brar LS. Numerical investigations of the flow-field inside cyclone separators with different cylinder-to-cone ratios using large-eddy simulation. Sep Purif Technol. 2020;249(11):117149. doi:10.1016/j.seppur.2020.117149.
14. Xie CD, Song CJ, Gao L, He ZK, Chen DY. Comparative analysis of cyclone separators used in grinding systems. China Cem. 2024(1):67–70. (In Chinese). doi:10.3969/j.issn.1671-8321.2024.01.017.
15. Zhang R, Yang J, Han S, Hao X, Guan G. Improving advantages and reducing risks in increasing cyclone height via an apex cone to grasp *vortex end*. Chin J Chem Eng. 2023;54(11):136–43. doi:10.1016/j.cjche.2022.04.014.
16. Erol HI, Turgut O, Unal R. Experimental and numerical study of Stairmand cyclone separators: a comparison of the results of small-scale and large-scale cyclones. Heat Mass Transf. 2019;55(8):2341–54. doi:10.1007/s00231-019-02589-y.
17. Peng L, Shi ZS, Dong F. Structure optimization of cyclone separator based on CFD-DPM. Power Gener Technol. 2021;42(3):343–9. (In Chinese). doi:10.12096/j.2096-4528.pgt.20043.
18. De Souza FJ, De Vasconcelos Salvo R, De Moro Martins D. Effects of the gas outlet duct length and shape on the performance of cyclone separators. Sep Purif Technol. 2015;142(2006):90–100. doi:10.1016/j.seppur.2014.12.008.
19. Zhang K, Yan Z, Sun Z, Yang H, Yang G. Performance evaluation and prediction model for novel elliptical cyclone separators. Sep Purif Technol. 2025;354(9):128888. doi:10.1016/j.seppur.2024.128888.
20. Zhang G, Chen G, Yan X. Evaluation and improvement of particle collection efficiency and pressure drop of cyclones by redistribution of dustbins. Chem Eng Res Des. 2018;139:52–61. doi:10.1016/j.cherd.2018.09.021.
21. Si D, Yan Z, Lu C. Performance experiments and pressure drop prediction modelling of an energy-saving cyclone separator. Fuel. 2024;372:132165. doi:10.1016/j.fuel.2024.132165.
22. Bernardo S, Peres AP, Mori M. Computational study of cyclone flow fluid dynamics using a different inlet section angle. Therm Eng. 2005;4(1):18. doi:10.5380/reterm.v4i1.3543.
23. Brar LS, Sharma RP, Elsayed K. The effect of the cyclone length on the performance of Stairmand high-efficiency cyclone. Powder Technol. 2015;286(11):668–77. doi:10.1016/j.powtec.2015.09.003.
24. Xiao B, Wang X, Song YY, Zhang B, Wu SK. Research and numerical simulation on gas solid flow characteristics of biomass dual fluidized bed. Acta Energiae Solaris Sin. 2024;45(3):133–8. (In Chinese). doi:10.19912/j.0254-0096.tynxb.2022-1768.

25. Zhang AQ. Numerical simulation study on the effects of arrangement patterns on internal flow field and crossflow back-mixing in parallel separators. Ind Heat. 2021;50(5):27–32. (In Chinese). doi:10.3969/j.issn.1002-1639.2021.05.008.
26. Emami F, Rostampour V, Rezvanivand Fanaei A, Feyzollahzadeh M, Qarachoboogh AF. A numerical assessment to select the optimal geometry of a specific cyclone separator of wheat flour processing. J Food Process Eng. 2024;47(2):e14555. doi:10.1111/jfpe.14555.
27. Jiang H, Xie YT, Liu HY, Niu JT. Numerical simulation study on the enhancement of cyclone separator in CFB boilers. Electr Power Technol Environ Prot. 2024;40(1):87–94. (In Chinese). doi:10.19944/j.eptep.1674-8069.2024.01.011.
28. Chu MH, Diao YF, Zhang LA, Zhuang JW. Numerical simulation of the effects of different fiber layer arrangements on PM2.5 capture performance. J Chem Eng China. 2021;21(5):541–9. doi:10.12034/j.issn.1009-606X.220152.
29. Babaoğlu NU, Parvaz F, Foroozesh J, Hosseini SH, Ahmadi G, Elsayed K. Geometry optimization of axial cyclone for high performance and low acoustic noise. Powder Technol. 2023;427:118738. doi:10.1016/j.powtec.2023.118738.
30. Gao SL, Ma XY, Jiang N. Yan-Zhu: the fascinating role of flow transport. Mech Pract. 2024;46(5):1113–7. doi:10.6052/1000-0879-24-265.
31. Xiang XD. Modern dust control theory and technology. Beijing, China: Metallurgical Industry Press; 2002. (In Chinese).
32. Cao G, Sun GG, Zhang YG, Yuan SW, Wu S. Influence of hopper coke collector on the performance and flow field of cyclone separators in a fluid catalytic cracking unit. Pet Refin Petrochem Technol. 2024;55(11):84–9. doi:10.3969/j.issn.1005-2399.2024.11.021.
33. Zhang H, Guo H, He XJ, Chang BB, Geng F, Chen X. Numerical simulation of dust capture characteristics in a micro-cyclone using CFD-DPM. China Saf Sci J. 2025;21(3):113–8. (In Chinese). doi:10.11731/j.issn.1673-193x.2025.03.014.
34. Wasilewski M, Ligus G, Brar LS. Investigations of the flow phenomena inside square cyclone separators with different prismatic heights. Sep Purif Technol. 2025;362:131724. doi:10.1016/j.seppur.2025.131724.
35. Kumar M, Vanka SP, Banerjee R, Mangadoddy N. Dominant modes in a gas cyclone flow field using proper orthogonal decomposition. Ind Eng Chem Res. 2022;61(6):2562–79. doi:10.1021/acs.iecr.1c03357.
36. Ma L, Zhao Z, Tian C, Wang H, Liu Y. Soot elimination and heat recovery of industrial flue gas by heterogeneous condensation. Sci Rep. 2020;10(1):2929. doi:10.1038/s41598-020-59833-3.
37. Nwokolo N, Mamphweli S, Makaka G. An investigation into heat recovery from the surface of a cyclone dust collector attached to a downdraft biomass gasifier. Appl Therm Eng. 2016;98(6):1158–64. doi:10.1016/j.applthermaleng.2016.01.014.
38. Wasilewski M. Analysis of the effects of temperature and the share of solid and gas phases on the process of separation in a cyclone suspension preheater. Sep Purif Technol. 2016;168:114–23. doi:10.1016/j.seppur.2016.05.033.
39. Nakhaei M, Lu B, Tian Y, Wang W, Dam-Johansen K, Wu H, et al. CFD modeling of gas-solid cyclone separators at ambient and elevated temperatures. Processes. 2020;8(2):228. doi:10.3390/pr8020228.
40. Zhang Y, Yu G, Jin R, Chen X, Dong K, Jiang Y, et al. Investigation into water vapor and flue gas temperatures on the separation capability of a novel cyclone separator. Powder Technol. 2020;361:171–8. doi:10.1016/j.powtec.2019.09.048.
41. Zhang R, Wu H, Si X, Zhao L, Yang L. Improving the removal of fine particulate matter based on heterogeneous condensation in desulfurized flue gas. Fuel Process Technol. 2018;174(2):9–16. doi:10.1016/j.fuproc.2018.01.015.
42. Liang Y, Cheng T, Li Q, Liu J, Li Q, Li J, et al. CFD-DEM simulation of cyclone self-rotation drying: particle high-speed self-rotation and heat transfer. Energy. 2024;290:130277. doi:10.1016/j.energy.2024.130277.
43. Li S, Li J, Xiao Y, Ma H, Chen Y, Jiang X, et al. Separation and recovery of waste heat from millimeter-sized blast furnace slag in cyclone separators. Sep Purif Technol. 2025;367:132908. doi:10.1016/j.seppur.2025.132908.
44. He Y, Dianyu E, Jiang Z. Particle motion and gas-solid heat exchange enhancement in rotary drums with aligned/separated flight. Processes. 2025;13(5):1594. doi:10.3390/pr13051594.
45. Szekely J, Carr R. Heat transfer in a cyclone. Chem Eng Sci. 1966;21(12):1119–32. doi:10.1016/0009-2509(66)85033-9.

46. Zhu LT, Liu YX, Luo ZH. An enhanced correlation for gas-particle heat and mass transfer in packed and fluidized bed reactors. Chem Eng J. 2019;374:531–44. doi:10.1016/j.cej.2019.05.194.
47. Rubio-López O, Montes-Rodríguez JJ, Rodríguez-Morales E, Montoya-Santiyanes LA. Particulate filtration by cryogenic condensation using a high efficiency Stairmand cyclone separator. Sep Purif Technol. 2024;342(20):126902. doi:10.1016/j.seppur.2024.126902.
48. Wang B, Liu H, Zhou C, Huo H, Dong K, Jiang Y. Enhancing the collection efficiency of a gas cyclone with atomization and electrostatic charging. Powder Technol. 2020;364:562–71. doi:10.1016/j.powtec.2020.01.062.
49. Zhao B, Su Y, Zhang J. Simulation of gas flow pattern and separation efficiency in cyclone with conventional single and spiral double inlet configuration. Chem Eng Res Des. 2006;84(12):1158–65. doi:10.1205/cherd06040.
50. Shin MS, Kim HS, Jang DS, Chung JD, Bohnet M. A numerical and experimental study on a high efficiency cyclone dust separator for high temperature and pressurized environments. Appl Therm Eng. 2005;25(11–12):1821–35. doi:10.1016/j.applthermaleng.2004.11.002.
51. Zhao J, Li B, Yao Y, Wang Z, Wei X, Li S. Numerical simulation of the flow and heat transfer in novel circumfluent cyclone separator during high-temperature converter gas recovery. Front Heat Mass Transf. 2025;23(1):163–84. doi:10.32604/fhmt.2024.059740.
52. Mariani F, Risi F, Grimaldi CN. Separation efficiency and heat exchange optimization in a cyclone. Sep Purif Technol. 2017;179(2):393–402. doi:10.1016/j.seppur.2017.02.024.
53. Xu S, Xie J, Mei S, He F, Li R, Deng Y, et al. Numerical simulation of gas-solid two-phase heat transfer in a Kaolin cyclone cooling system. Energies. 2023;16(9):3744. doi:10.3390/en16093744.
54. Dias DR, Ullmann G, Oliveira Silva D, Vieira LGM. Thermal performance of a psychrometric cooling system using cyclone fluid dynamics. Chem Eng Res Des. 2024;203:333–45. doi:10.1016/j.cherd.2024.01.058.
55. Fatahian H, Fatahian E, Erfani R. Square cyclone separator: performance analysis optimization and operating condition variations using CFD-DPM and taguchi method. Powder Technol. 2023;428(1):118789. doi:10.1016/j.powtec.2023.118789.
56. Soliman MM, El-shaer Y, Elsayed K, Ibrahim MA. Performance enhancement of gas cyclone with streamlined ports using CFD simulations. J Eng Appl Sci. 2025;72(1):4. doi:10.1186/s44147-024-00575-8.
57. Wang YB, Zhao BD, Xu F, Lan B, Wang JW. Full-Loop simulation of a circulating fluidized bed based on the structured two-fluid model. Chem Eng Prog. 2025;44(8):4500–12. doi:10.16085/j.issn.1000-6613.2025-0147.
58. Zhang F, Zirwes T, Habisreuther P, Zarzalis N, Bockhorn H, Trimis D. Numerical computation of turbulent flow fields in a fan-stirred combustion bomb. Combust Sci Technol. 2021;193(4):594–610. doi:10.1080/00102202.2019.1665520.
59. Vermande Paganel T, Fabrice Alban E, Cyrille MA, Ngayihi Abbe CV. CFD simulation of an industrial dust cyclone separator: a comparison with empirical models: the influence of the inlet velocity and the particle size on performance factors *in situ* ation of high concentration of particles. J Eng. 2024;2024(1):5590437. doi:10.1155/2024/5590437.
60. Sun X, Shen W, Fan J, Vogel-Heuser B, Zhang C. An improved non-dominated sorting genetic algorithm II for distributed heterogeneous hybrid flow-shop scheduling with blocking constraints. J Manuf Syst. 2024;77:990–1008. doi:10.1016/j.jmsy.2024.10.018.
61. Balestrin E, Decker RK, Noriler D, Bastos JCSC, Meier HF. An alternative for the collection of small particles in cyclones: experimental analysis and CFD modeling. Sep Purif Technol. 2017;184:54–65. doi:10.1016/j.seppur.2017.04.023.
62. De Souza FJ, De Vasconcelos Salvo R, De Moro Martins DA. Large eddy simulation of the gas-particle flow in cyclone separators. Sep Purif Technol. 2012;94:61–70. doi:10.1016/j.seppur.2012.04.006.
63. Anderson JD, Wendt J. Computational fluid dynamics: an introduction. 3rd ed. Berlin/Heidelberg, Germany: Springer; 2009.
64. Bergman TL, Lavine A, Incropera FP, DeWitt DP. Fundamentals of heat and mass transfer. 7th ed. Hoboken, NJ, USA: John Wiley & Sons; 2011.

65. Parker MJ, Savory E, Straatman AG. Statistically accurate discrete phase modelling of particle cloud generation using aggregate steady random particle injection. Powder Technol. 2022;411(5):117959. doi:10.1016/j.powtec.2022.117959.
66. Abouali O, Nikbakht A, Ahmadi G, Saadabadi S. Three-dimensional simulation of Brownian motion of nanoparticles in aerodynamic lenses. Aerosol Sci Technol. 2009;43(3):205–15. doi:10.1080/02786820802587888.
67. Maxey MR, Riley JJ. Equation of motion for a small rigid sphere in a nonuniform flow. Phys Fluids. 1983;26(4):883–9. doi:10.1063/1.864230.
68. Gopalakrishnan B, Saravana Kumar G, Prakash KA. Parametric analysis and optimization of gas-particle flow through axial cyclone separator: a numerical study. Adv Powder Technol. 2023;34(2):103959. doi:10.1016/j.apt.2023.103959.
69. Alletto M, Breuer M. One-way, two-way and four-way coupled LES predictions of a particle-laden turbulent flow at high mass loading downstream of a confined bluff body. Int J Multiph Flow. 2012;45:70–90. doi:10.1016/j.ijmultiphaseflow.2012.05.005.
70. Procedure for estimation and reporting of uncertainty due to discretization in CFD applications. J Fluids Eng. 2008;130(7):078001. doi:10.1115/1.2960953.
71. Meana-Fernández A, Fernández Oro JM, Argüelles Díaz KM, Galdo-Vega M, Velarde-Suárez S. Application of Richardson extrapolation method to the CFD simulation of vertical-axis wind turbines and analysis of the flow field. Eng Appl Comput Fluid Mech. 2019;13(1):359–76. doi:10.1080/19942060.2019.1596160.
72. Zigh G, Solis J. Computational fluid dynamics best practice guidelines for dry cask applications: final report (NUREG-2152). Washington, DC, USA: U.S. Nuclear Regulatory Commission; 2013 [cited 2026 Jan 1]. Available from: https://www.nrc.gov/reading-rm/doc-collections/nuregs/staff/sr2152/index.html.
73. Dong Y, Du L, Li G. Hybrid ship design optimization framework integrating a dual-mode CFD-surrogate mechanism. Appl Sci. 2025;15(19):10318. doi:10.3390/app151910318.
74. Mao R, Lan Y, Liang L, Yu T, Mu M, Leng W, et al. Rapid CFD prediction based on machine learning surrogate model in built environment: a review. Fluids. 2025;10(8):193. doi:10.3390/fluids10080193.
75. Koziel S, Leifsson L. Surrogate-based aerodynamic shape optimization by variable-resolution models. AIAA J. 2013;51(1):94–106. doi:10.2514/1.j051583.
76. Guo M, Le DK, Sun X, Yoon JY. Multi-objective optimization of a novel *vortex* finder for performance improvement of cyclone separator. Powder Technol. 2022;410(5):117856. doi:10.1016/j.powtec.2022.117856.
77. Wang Z, Yang Y, Wang L. Projection generalized correntropy twin support vector regression. Artif Intell Rev. 2024;57(8):223. doi:10.1007/s10462-024-10856-6.
78. Hu Y, Lu Z, Wei N, Jiang X. Importance sampling enhanced by adaptive two-stage Kriging model and active subspace for analyzing rare probability with high dimensional input vector. Reliab Eng Syst Saf. 2024;245:110019. doi:10.1016/j.ress.2024.110019.
79. Nan H, Liang H, Di H, Li H. A gradient-assisted learning strategy of Kriging model for robust design optimization. Reliab Eng Syst Saf. 2024;244:109944. doi:10.1016/j.ress.2024.109944.
80. Zhu C, Mou X, Bao Z. Optimization of tree-shaped fin structures towards enhanced discharging performance of metal hydride reactor for thermochemical heat storage based on entransy theory. Renew Energy. 2024;220:119585. doi:10.1016/j.renene.2023.119585.
81. Yang F, Feng H, Wu L, Zhang Z, Wang J. Performance prediction and parameters optimization of an opposed-piston free piston engine generator using response surface methodology. Energy Convers Manag. 2023;295(66):117633. doi:10.1016/j.enconman.2023.117633.
82. Haddad HZ, Mohamed MH, Shabana YM, Elsayed K. Optimization of Savonius wind turbine with additional blades by surrogate model using artificial neural networks. Energy. 2023;270(1):126952. doi:10.1016/j.energy.2023.126952.
83. Ghafariasl P, Mahmoudan A, Mohammadi M, Nazarparvar A, Hoseinzadeh S, Fathali M, et al. Neural network-based surrogate modeling and optimization of a multigeneration system. Appl Energy. 2024;364(12):123130. doi:10.1016/j.apenergy.2024.123130.

84. Hou CKJ, Behdinan K. Dimensionality reduction in surrogate modeling: a review of combined methods. Data Sci Eng. 2022;7(4):402–27. doi:10.1007/s41019-022-00193-5.
85. Guo Y, Mahadevan S, Matsumoto S, Taba S, Watanabe D. Investigation of surrogate modeling options with high-dimensional input and output. AIAA J. 2023;61(3):1334–48. doi:10.2514/1.j061901.
86. Mukhtar A, Yasir ASHM, Nasir MFM. A machine learning-based comparative analysis of surrogate models for design optimisation in computational fluid dynamics. Heliyon. 2023;9(8):e18674. doi:10.1016/j.heliyon.2023.e18674.
87. Zhao B, Chen WN, Wei FF, Liu X, Pei Q, Zhang J. PEGA: a privacy-preserving genetic algorithm for combinatorial optimization. IEEE Trans Cybern. 2024;54(6):3638–51. doi:10.1109/TCYB.2023.3346863.
88. Zhang T, Chen L, Wang J. Multi-objective optimization of elliptical tube fin heat exchangers based on neural networks and genetic algorithm. Energy. 2023;269(1):126729. doi:10.1016/j.energy.2023.126729.
89. Altanany MY, Badawy M, Ebrahim GA, Ehab A. Modeling and optimizing linear projects using LSM and non-dominated sorting genetic algorithm (NSGA-II). Autom Constr. 2024;165:105567. doi:10.1016/j.autcon.2024.105567.
90. Safikhani H. Modeling and multi-objective Pareto optimization of new cyclone separators using CFD, ANNs and NSGA II algorithm. Adv Powder Technol. 2016;27(5):2277–84. doi:10.1016/j.apt.2016.08.017.
91. Yang J, Zou J, Yang S, Hu Y, Zheng J, Liu Y. A particle swarm algorithm based on the dual search strategy for dynamic multi-objective optimization. Swarm Evol Comput. 2023;83(5):101385. doi:10.1016/j.swevo.2023.101385.
92. Yang Z, Guo P, Wang L, Hao Q. Multi-objective optimization analysis of hydrogen internal combustion engine performance based on game theory. Appl Energy. 2024;374(40):123946. doi:10.1016/j.apenergy.2024.123946.
93. Zhang W, Zhang L, Yang J, Hao X, Guan G, Gao Z. An experimental modeling of cyclone separator efficiency with PCA-PSO-SVR algorithm. Powder Technol. 2019;347(12):114–24. doi:10.1016/j.powtec.2019.01.070.
94. Zhou T, Han X, Wang L, Gan W, Chu Y, Gao M. A multiobjective differential evolution algorithm with subpopulation region solution selection for global and local Pareto optimal sets. Swarm Evol Comput. 2023;83(5):101423. doi:10.1016/j.swevo.2023.101423.
95. Wu L, Zhao X, Ye L, Qiao Z, Zuo X. Fuzzy clustering-based large-scale multimodal multi-objective differential evolution algorithm. Swarm Evol Comput. 2025;93(4):101856. doi:10.1016/j.swevo.2025.101856.
96. Tian M, Yan X, Gao X. An enhanced adaptive differential evolution algorithm with dual performance evaluation metrics for numerical optimization. Swarm Evol Comput. 2024;84(4):101454. doi:10.1016/j.swevo.2023.101454.
97. Banh QN, Truong PD, Ho MT. Multi-objective optimization of water-assisted injection molding using machine learning and CFD simulations. Results Eng. 2025;28:107981. doi:10.1016/j.rineng.2025.107981.
98. Guan B, Li J. Multi-objective shape optimization method for underwater dam defect detection ROV based on response surface model and NSGA-III algorithm. Ocean Eng. 2026;343:123614. doi:10.1016/j.oceaneng.2025.123614.
99. Li J, Wang T, Zhang L, Chang J, Song Z, Ma C. Multi-objective optimization of axial-flow-type gas-particle cyclone separator using response surface methodology and computational fluid dynamics. Atmos Pollut Res. 2020;11(9):1487–99. doi:10.1016/j.apr.2020.06.002.
100. Ning N, Lai XD, Ye DX. Geometric parameter optimization of a guide-vane separator for pressure drop reduction. Therm Power Eng. 2020;35(6):170–6. doi:10.16146/j.cnki.rndlgc.2020.06.024.
101. Pandey S, Wasilewski M, Mukhopadhyay A, Prakash O, Ahmad A, Brar LS, et al. Multi-objective optimization of cyclone separators based on geometrical parameters for performance enhancement. Appl Sci. 2024;14(5):2034. doi:10.3390/app14052034.
102. Sun X, Yoon JY. Multi-objective optimization of a gas cyclone separator using genetic algorithm and computational fluid dynamics. Powder Technol. 2018;325(1973):347–60. doi:10.1016/j.powtec.2017.11.012.
103. Deng Y, Yu B, Sun D. Multi-objective optimization of guide vanes for axial flow cyclone using CFD, SVM, and NSGA II algorithm. Powder Technol. 2020;373(2):637–46. doi:10.1016/j.powtec.2020.06.078.
104. Elsayed K. Optimization of the cyclone separator geometry for minimum pressure drop using Co-Kriging. Powder Technol. 2015;269(22):409–24. doi:10.1016/j.powtec.2014.09.038.
105. Li W, Huang Z, Li G. Improvement of the cyclone separator performance by the wedge-shaped roof: a multi-objective optimization study. Chem Eng Sci. 2023;268(3):118404. doi:10.1016/j.ces.2022.118404.

106. Cao G, Sun G, Yuan S, Yue Y, Wu Y. Multiobjective optimization of spiral guide vanes for boosting separation performance of cyclone separators. Ind Eng Chem Res. 2024;63(20):9162–75. doi:10.1021/acs.iecr.4c00172.
107. Mahmoodabadi MJ, Bagheri A, Abedzadeh Maafi R, Hoseini GR. Pareto optimal design of square cyclone separators using a novel multi-objective optimization algorithm. Trans Inst Meas Control. 2013;35(3):289–300. doi:10.1177/0142331212444154.
108. Dehdarinejad E, Bayareh M. Performance analysis of a novel cyclone separator using RBFNN and MOPSO algorithms. Powder Technol. 2023;426(4):118663. doi:10.1016/j.powtec.2023.118663.
109. Elsayed K, Lacor C. Multi-objective surrogate based optimization of gas cyclones using support vector machines and CFD simulations. In: Application of surrogate-based global optimization to aerodynamic design. Berlin/Heidelberg, Germany: Springer; 2016. p. 59–72. doi:10.1007/978-3-319-21506-8_4.
110. Izadi A, Kashani E, Mohebbi A. Combining 10 meta-heuristic algorithms, CFD, DOE, MGGP and PROMETHEE II for optimizing Stairmand cyclone separator. Powder Technol. 2021;382(2):70–84. doi:10.1016/j.powtec.2020.12.056.
111. Singh P, Couckuyt I, Elsayed K, Deschrijver D, Dhaene T. Shape optimization of a cyclone separator using multi-objective surrogate-based optimization. Appl Math Model. 2016;40(5–6):4248–59. doi:10.1016/j.apm.2015.11.007.
112. Sun X, Kim S, Yang SD, Kim HS, Yoon JY. Multi-objective optimization of a Stairmand cyclone separator using response surface methodology and computational fluid dynamics. Powder Technol. 2017;320(1):51–65. doi:10.1016/j.powtec.2017.06.065.
113. Liang HQ, Shi WW, Zhang XR, Yu FR. Multi-objective optimization for structural parameters of guide vane cyclone separator based on improved PSO algorithm. Mach Tool Hydraul. 2023;51(3):180–6. (In Chinese). doi:10.3969/j.issn.1001-3881.2023.03.031.
114. Elsayed K, Lacor C. Modeling and Pareto optimization of gas cyclone separator performance using RBF type artificial neural networks and genetic algorithms. Powder Technol. 2012;217(8):84–99. doi:10.1016/j.powtec.2011.10.015.
115. Hatami M, Ganji DD, Gorji-Bandpy M. Experimental and thermodynamical analyses of the diesel exhaust *vortex generator* heat exchanger for optimizing its operating condition. Appl Therm Eng. 2015;75(9):580–91. doi:10.1016/j.applthermaleng.2014.09.058.